Optically excited near-surface phonons of TiO2 (110) observed by fourth-order coherent Raman spectroscopy

Nomoto, Tomonori

Sasahara, Akira

Onishi, Hiroshi

Optically excited near-surface phonons of TiO₂ (110) observed by fourth-order coherent Raman spectroscopy

Tomonori Nomoto (野本知理),[1,2,a)] Akira Sasahara (笹原亮),[2,3,b)] and Hiroshi Onishi (大西洋)[3]

[1]*Molecular Photoscience Research Center, Kobe University, Rokkodai, Nada, Kobe 657-8501, Japan*
[2]*Core Research for Evolutional Science and Technology, Japan Science and Technology Agency, Honmachi, Kawaguchi 332-0012, Japan*
[3]*Department of Chemistry, Graduate School of Science, Kobe University, Rokkodai, Nada, Kobe 657-8501, Japan*

We observed the fourth-order and third-order optical responses in the time domain on a TiO₂ (110) surface covered with trimethyl acetates. Coherent vibrations assignable to near-surface phonon modes were present at 179, 191, 359, 440, 507, 609, and 823 cm^{-1} in the fourth-order responses. The amplitude and phase of each mode were determined with different azimuths and polarizations of pump and probe light pulses. Vibrational assignments and possible mechanisms to excite the vibrations were discussed. © *2009 American Institute of Physics*. [DOI: 10.1063/1.3207947]

I. INTRODUCTION

Interfaces have different characteristics from the bulk substrates. The loss of the translational symmetry of the crystal causes the depth dependent distribution of vibrational resonance as observed as surface phonon modes.[1] Adsorbed species further affect the surface modes. However, in many cases, the optical responses of an interface are overridden by responses of the bulk because the spatial resolution is limited by the wavelength of the light probe. For reducing the bulk contribution to the signal, several interface-sensitive methods have been developed. For vibrational spectroscopy, high-resolution electron energy loss spectroscopy,[2] infrared reflection absorption spectroscopy,[3] helium atom scattering,[4] and sum frequency generation[5–7] are frequently used.

Fourth-order coherent Raman (FR) spectroscopy, which has been developed recently, is a new alternative of interface-selective vibrational spectroscopy.[7–14] It is an even-order nonlinear optical spectroscopy sensitive to interfaces on centrosymmetric substrates. A merit of FR spectroscopy is that the FR process does not require an infrared light source. The infrared-free measurement of FR spectroscopy enables observation of interfaces buried in media with intense infrared absorption such as water. FR spectra were reported on vacuum-solid,[7,8] air-solid,[10,15] solid-solid,[9] air-liquid,[12,14,16] liquid-liquid,[11] and liquid-solid interfaces.[16,17] Another merit of FR spectroscopy is sensitivity to low-frequency vibrations. Using time-domain detection of impulsively excited vibrational coherences with 20 fs pulses, vibrations below 1000 cm^{-1} are observable.

We have examined the fourth-order optical response of a TiO₂ (110) surface covered with an organic compound[10,15] to simulate TiO₂-based photocatalysts operated in the air. A number of vibrational bands were observed and expected to be phonon modes perturbed by the surface. However, the origin of the vibrations was still ambiguous although the observed modes in FR spectroscopy had similar frequency to bulk or surface optical phonon mode of TiO₂. In the current study, the amplitude and phase of the bands are systematically examined with different azimuths and polarizations of light pulses. Related bulk phonon modes are carefully identified on the same surface using the third-order response. Possible excitation mechanisms of the vibrational coherence are discussed on these experimental results.

II. EXPERIMENTAL

A TiO₂ (110) surface was prepared in an ultrahigh vacuum chamber. A one-side polished TiO₂ (110) crystal (10×10×0.5 mm³, Shinkosha, Japan) was Ar⁺-ion sputtered at room temperature and annealed at 1000 K in a vacuum of 1×10^{-7} Pa. The sputter-annealed surface was reduced to be blue in color and presented the (1×1) pattern in low-energy electron diffraction. The TiO₂ surface was then exposed to trimethyl acetic acid ((CH₃)₃CCOOH) vapor at 2×10^{-5} Pa for 60 s at room temperature. A (2×1) pattern was observed on the exposed surface as evidence of a long-range ordered monolayer of trimethyl acetate (TMA). The TMA monolayer terminated with a hydrophobic functional group offers surface stability in the air.[6,10] The TMA-covered TiO₂ (110) was removed from the vacuum for FR measurements.

Our measurement system is shown in Fig. 1(a). The light source was a noncollinear optical parametric amplifier (NOPA: TOPAS-*white*, Quantronix) pumped by a Ti:sapphire regenerative amplifier (Hurricane, Spectra Physics, 1 kHz repetition rate). The output of the NOPA (620 nm) was separated into pump and probe pulses. A zero-order quartz half-wave plate was inserted into the pump light path for adjusting the polarization. An optical delay was inserted into the
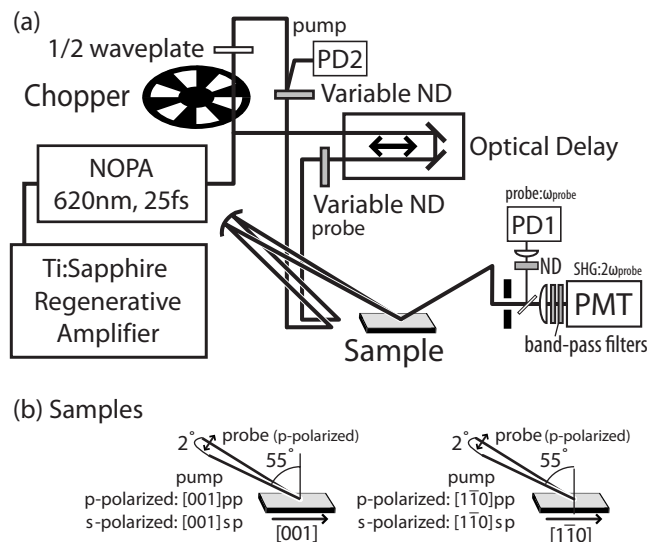
FIG. 1. (a) Experimental setup for the fourth-order and third-order optical responses. (b) Sample orientation and input polarization.

probe light path. Variable neutral density filters (VND-50U, Sigma Koki) were used to adjust the pump and probe intensities. The pump and probe pulses (8 mJ/cm^2 each) were focused on the TiO$_2$ surface by a concave mirror. The second harmonic (SH) light generated by the probe pulses was filtered with two filters (U330 filter with coating, Asahi Spectra) and detected by a photomultiplier tube (PMT) (H5784-03, Hamamatsu Photonics). The SH generation of TiO$_2$ surfaces is well studied.[18] The reflection of the fundamental probe pulses was simultaneously detected by a photodiode (PD1: S1336-44BQ, Hamamatsu Photonics) coupled with current preamplifiers (LI-76, NF Corporation). PMT and PD1 outputs were integrated by a boxcar integrator (SR245, Stanford Research System) and analog-to-digital converted pulse by pulse (PCI-6251, National Instruments). The pump pulses were modulated at 500 Hz with a synchronous mechanical chopper (3501, New Focus), and the signals with pump-on and pump-off were separately accumulated. The pump pulses reflected from VND were monitored by another photodiode (PD2) for determining whether the pump was on or off. The center wavelength of the pulses was 620 nm, and the time width was 25 fs as the cross correlation between the pump and probe pulses on the sample surface. The incident angle of both the pump and probe pulses was 55° from the surface normal with a crossing angle of 2°. Sample orientations were [001] and [1$\bar{1}$0], where (1$\bar{1}$0) and (001) planes bisect the crossing angle of pump and probe pulses. Probe pulses were p-polarized for all measurements, while s and p-polarized pulses were used as pump pulses with each sample orientation [Fig. 1(b)]. The time delay was scanned from −0.3 to 3 ps at a 6 fs step for the [001] and [1$\bar{1}$0] orientations with p-polarized pump excitation ([001]pp and [1$\bar{1}$0]pp each) and from −0.3 to 1.5 ps at a 6 fs step for the [001] and [1$\bar{1}$0] orientations with s-polarized pump excitation ([001]sp and [1$\bar{1}$0]sp). 108 000, 344 000, 238 000, and 206 000 pulses were integrated to obtain the SH and funda-

mental light intensity profiles for the [001]pp, [1$\bar{1}$0]pp, [001]sp, and [1$\bar{1}$0]sp setups, respectively.

III. RESULTS

A. Separation of the fourth-order responses from the time-resolved second harmonic intensity

The time profile of the SH intensity of probe pulses for the TMA covered TiO$_2$ (110) of the [001]pp setup is shown in Fig. 2(a). $I(2\omega)/I_0(2\omega)$ is the pumped SH intensity relative to the pump-free SH intensity. The electric field of the observed SH is the summation of the periodically modulated field $E_{mod}(2\omega, t_d)$ and the nonperiodically modulated field $E_{non}(2\omega, t_d)$. Because the periodic modulations are generated from pump-induced vibrational coherences, E_{mod} is expressed as the sum of periodic oscillations as

$$E_{mod}(2\omega, t_d) \propto \chi^{(4)}(t_d)$$
$$\propto \sum_v A_v \exp(i(\omega_v t_d + \varphi_v))\exp(-t_d/T_v), \quad (1)$$

where A_v, ω_v, φ_v, T_v, and t_d are the amplitude, frequency, phase, dephasing time of each vibrational mode, and time delay of the probe pulse. $\chi^{(4)}$ is the fourth-order response of the interface. The intensity of observed SH is

$$I(2\omega, t_d) \propto |E_{non}(2\omega, t_d) + E_{mod}(2\omega, t_d)\exp(i\varphi_{non})|^2, \quad (2)$$

where φ_{non} represents the relative phase between $E_{mod}(2\omega, t_d)$ and the local oscillator $E_{non}(2\omega, t_d)$. When $|E_{non}(2\omega, t_d)| \gg |E_{mod}(2\omega, t_d)|$, the modulation amplitude is proportional to the heterodyned oscillatory component, which is

$$E_{non}^*(2\omega, t_d)E_{mod}(2\omega, t_d)\exp(i\varphi_{non})$$
$$\propto \sum_v A_v \exp(i(\omega_v t_d + \varphi_v + \varphi_{non}))\exp(-t_d/T_v). \quad (3)$$

On one-photon resonant dye solution interfaces, cosine-type oscillation with $\varphi_v + \varphi_{non} = 0°$ is reported.[11,12]

For obtaining the oscillatory component of the FR signal, a nonoscillatory decay of the SH intensity was fitted by a mixed function composed of one Gaussian function, one or two Gaussian convoluted exponential functions, and the Gaussian convoluted step function. The last component represents slow decay over 100 ps. The mixed function reproduced the whole nonoscillatory SH time profile well. The obtained time constants of the exponential decay were 160 fs and 1.2 ps with a full width at half maximum (FWHM) of the Gaussian function, 25 fs. The oscillatory FR component which remained after subtraction is shown in Fig. 2(b). To obtain the Fourier-transformed (FT) spectrum with a better signal-to-noise ratio, zero data were added to the end of the oscillatory FR component to 30 ps, and a Gaussian window function with 1 ps half width at half maximum (HWHM) was multiplied to the data before Fourier transformation. Multiplying the window function corresponds to a convolution of the FT spectrum with a Gaussian function having a FWHM of 15 cm^{-1}. The resulting FT spectrum is shown in Fig. 2(c), and it is essentially the same as the previously reported spectra.[10,15] The imaginary part represents sine
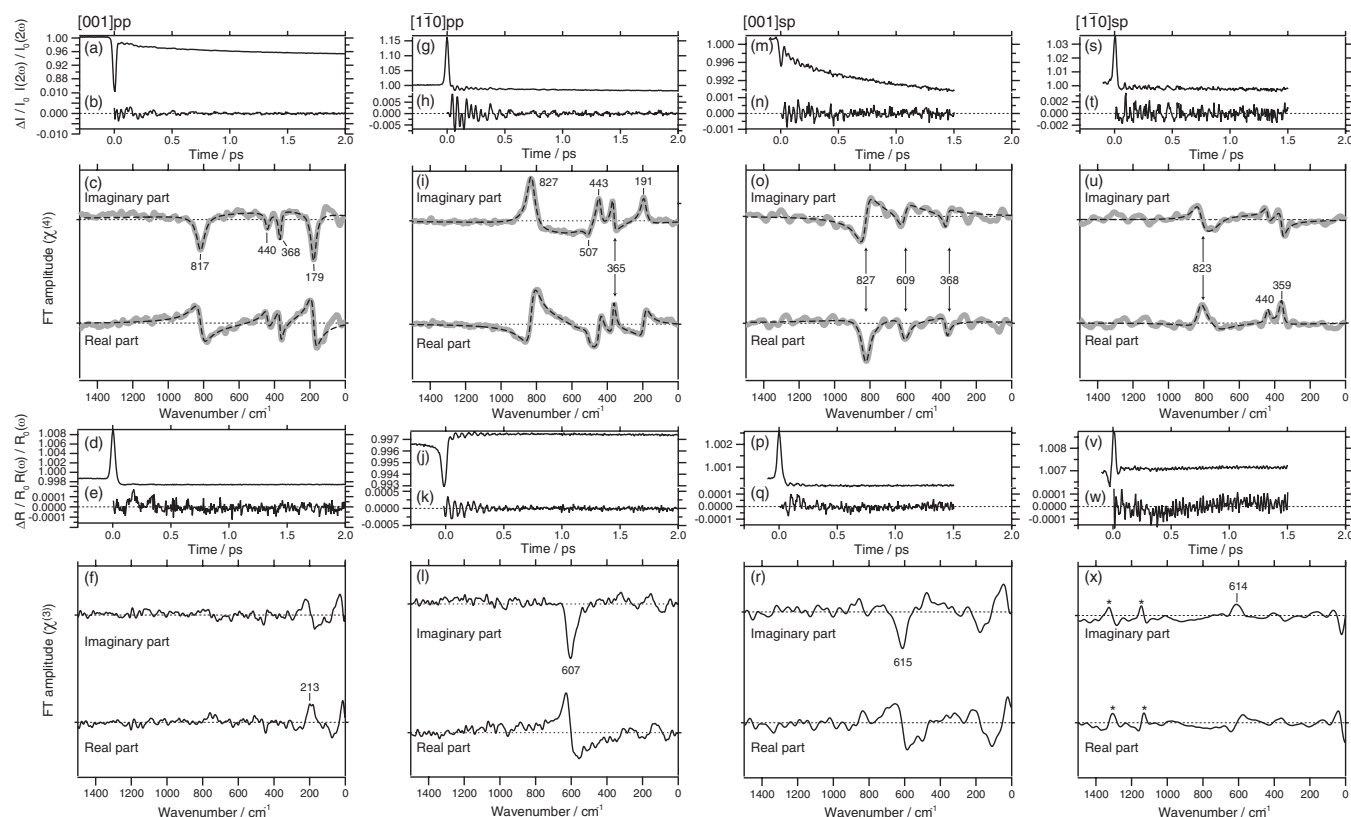
FIG. 2. Intensity changes in the reflected SH light from the TMA-covered TiO₂ (110) with (a) [001]pp, (g) [1̄10]pp, (m) [001]sp, and (s) [1̄10]sp geometries. The quantum beat component that was left after subtraction of the fitting curve for (b) [001]pp, (h) [1̄10]pp, (n) [001]sp, and (t) [1̄10]sp. FT spectra of the modulated component of SHG with (c) [001]pp, (i) [1̄10]pp, (o) [001]sp, and (u) [1̄10]sp. Intensity change in the fundamental light reflection for (d) [001]pp, (j) [1̄10]pp, (p) [001]sp, and (v) [1̄10]sp. The quantum beat component that was left after subtraction of the fitting curve for (e) [001]pp, (k) [1̄10]pp, (q) [001]sp, and (w) [1̄10]sp. FT spectra of modulated component of reflection, (f) [001]pp, (l) [1̄10]pp, (r) [001]sp, and (x) [1̄10]sp. Asterisks in (x) represent artifacts derived from laser instability.

components of the oscillation ($\varphi_v + \varphi_{non} = 90°$) and the real part represents cosine components of the oscillation ($\varphi_v + \varphi_{non} = 0°$).

B. Spectral fitting to the obtained FT spectra

For obtaining the wave number and the phase of vibrational coherences, the spectrum was fitted using the Lorentzian functions

$$S_{FRS}(\omega) = \sum_v \frac{A_v}{(\omega - \omega_v) + i\Gamma_v} \exp(i\theta_v), \quad (4)$$

where A_v, ω_v, Γ_v, and θ_v are the amplitude, center wave number, bandwidth, and phase of each mode. The phase is defined as $\theta_v = \varphi_v + \varphi_{non} + 90°$. Five Lorentzian functions were used to reproduce the spectrum. Four are for substantial vibrations of 817, 440, 368, and 179 cm⁻¹, while one at 325 cm⁻¹ represents the artifact derived from the fitting residue in the time-domain profile. The zero phase ($\theta_v = 0$) was initially assumed to minimize the number of fitting parameters. Three bands (817, 440, and 179 cm⁻¹) were fitted using $\theta_v = 0$, whereas finite phases were necessary for the other two bands to reproduce the observed spectrum. The obtained fitting parameters are shown in Table I(a) and the simulated spectrum is in Fig. 2(c).

The vibrational coherence is also projected on the intensity of the probe light reflected by the surface. $\chi^{(3)}$ governs this optical response. The time-domain profile of reflected probe pulses is shown in Fig. 2(d). R/R_0 is the reflection intensity relative to the pump-free intensity. The oscillatory component of R/R_0 [Fig. 2(e)] was FT to obtain a $\chi^{(3)}$ spectrum [Fig. 2(f)]. One peak present at 201 cm⁻¹ was fitted using Eq. (4) with the parameters in Table II. Structures below 100 cm⁻¹ are considered to be artifacts.

C. Azimuth and polarization dependence of the FR responses for TiO₂ (110)

The raw SH intensity obtained on the TMA-covered surface of the [1̄10]pp setup is shown in Fig. 2(g). The nonoscillatory component was fitted using a decay constant of 1.7 ps and a Gaussian FWHM of 29 fs. The oscillatory FR component and the FT spectrum are shown in Figs. 2(h) and 2(i). The obtained spectrum was fitted with the parameters in Table I(b). Six Lorentzian functions were required to fit [Table I(c)]. Five substantial bands (827, 507, 443, 365, and 191 cm⁻¹) were obtained. The obtained time profile of reflection of the probe pulses for the same sample is shown in Fig. 2(j). The oscillatory component of the reflection intensity and the $\chi^{(3)}$ spectrum are shown in Figs. 2(k) and 2(l) with parameters in Table II. A peak at 607 cm⁻¹ was ob-

TABLE I. Fitting parameters of FR spectra of the TiO_2 (110) surface covered by TMA with irradiation azimuth to (a) [001] direction with p-pump and p-probe, (b) [001] direction with s-pump and p-probe, (c) [1$\bar{1}$0] direction with p-pump and p-probe, and (d) [1$\bar{1}$0] direction with s-pump and p-probe.

(a) [001]pp			
ω_v/cm^{-1}	Γ_v/cm^{-1}	A_v	θ_v/deg
817	28	1.4	0 (fixed)
440	13	0.3	0 (fixed)
368	9	0.4	15
179	18	1.3	0 (fixed)
Baseline			
325	449	−5.6	14

(b) [001]sp			
ω_v/cm^{-1}	Γ_v/cm^{-1}	A_v	θ_v/deg
827	30	0.4	77
609	26	0.2	58
368	13	0.1	46
Baseline			
554	403	−0.7	−289

(c) [1$\bar{1}$0]pp			
ω_v/cm^{-1}	Γ_v/cm^{-1}	A_v	θ_v/deg
827	28	−4.2	15
507	24	0.8	0 (fixed)
443	17	−1.4	33
365	10	−0.8	52
191	20	−1.5	21
Baseline			
570	201	8.6	31

(d) [1$\bar{1}$0]sp			
ω_v/cm^{-1}	Γ_v/cm^{-1}	A_v	θ_v/deg
823	31	−1.1	50
440	12	−0.2	86
359	14	−0.5	110
Baseline			
739	84	1.5	61

served in the imaginary part. Structures below 200 cm^{-1} in the $\chi^{(3)}$ spectrum are considered to be artifacts.

The raw SH intensity obtained with the [001]sp setup is shown in Fig. 2(m). The nonoscillatory component was fitted using decay constants of 60 fs and 1.0 ps with a Gaussian FWHM of 28 fs. A Gaussian window function was multiplied with the oscillatory FR component and then FT. The oscillatory component of the SH intensity and the FT spec-

TABLE II. Fitting parameters of $\chi^{(3)}$ spectra of the TiO_2 (110) surface covered by TMA.

Azimuth and polarization	ω_v/cm^{-1}	Γ_v/cm^{-1}	A_v	θ_v/deg
[001] pp	201	19	−0.04	62
[001] sp	615	26	0.03	0 (fixed)
[1$\bar{1}$0]pp	607	23	0.16	0 (fixed)
[1$\bar{1}$0]sp	614	38	−0.05	0 (fixed)

trum are shown in Figs. 2(n) and 2(o). The HWHM of the window function was tuned to be 0.5 ps. The SH response pumped with the s-polarized pulses was observed up to 1.5 ps. The time width of the window function is appropriate with the 1.5 ps response. As a result, the FT spectrum of Fig. 2(o) was convoluted with a Gaussian function with 30 cm^{-1} FWHM. With the p-polarized pump pulses the SH response was traced up to 3 ps, where a wider window function was used.

The obtained spectrum was Lorentzian fitted with the parameters in Table I(b). Four Lorentzian functions were required for fitting and three substantial bands were obtained at 827, 609, and 368 cm^{-1}. The raw R/R_0, modulated component, and $\chi^{(3)}$ spectrum are shown in Figs. 2(p)–2(r) with the parameters in Table II. A peak at 615 cm^{-1} was observed in the imaginary part.

The raw SH intensity obtained with the [1$\bar{1}$0]sp setup is shown in Fig. 2(s). The nonoscillatory component was fitted using a decay constant of 2.3 ps and a Gaussian FWHM of 30 fs. The oscillatory FR component of the SH intensity and the FT spectrum are shown in Figs. 2(t) and 2(u). Four Lorentzian functions were required with the parameters in Table I(d). Three substantial bands (823, 440, and 359 cm^{-1}) were identified. The $\chi^{(3)}$ response of the surface is shown in Figs. 2(v)–2(x) and Table II. A peak at 614 cm^{-1} was present in the imaginary part.

IV. DISCUSSION

We observed seven phonon modes of TiO_2 in the $\chi^{(4)}$ response and two in the $\chi^{(3)}$ spectra. The molecular vibrations of TMA monolayer covering the surface were not observed because no electronic resonance could contribute to $\chi^{(4)}$ process for TMA, which has no absorption in fundamental and SH wavelength. The different numbers of the observed phonons reflect the different selection rules of the $\chi^{(3)}$ and $\chi^{(4)}$ processes. Because $\chi^{(3)}$ response is bulk sensitive, the two $\chi^{(3)}$ modes at 610 and 200 cm^{-1} represent bulk phonons. Lattice dynamics of bulk TiO_2 was reported by infrared,[19] Raman,[20] and neutron diffraction with phonon dispersion.[21] Based on the vibrational studies of TiO_2 crystals,[19–22] the mode at 610 cm^{-1} was assigned to a bulk phonon of A_{1g} symmetry. On the other hand, there is no fundamental tone of TiO_2 phonons at 200 cm^{-1}. An overtone or combination of lower-frequency phonons is a possible origin of this band.[20,23]

A. Possible excitation mechanisms

It is established with $\chi^{(3)}$ responses that the phase of vibrational coherence is sensitive to the time feature of the driving force.[24–27] When an impulsive force is present at the time origin, a sine-form coherence is generated. This is typically the case with impulsive stimulated Raman scattering (ISRS) off-resonant to electric transitions. A cosine-form coherence appears when a steplike force is applied. This is the case in the ISRS process with an electronic resonance when the imaginary part of the Raman tensor dominates coherent phonon generation.[27] There is also a transient depletion field screening (TDFS) (Ref. 24) and displacive excitation of co-

herent phonon (DECP) (Ref. [25]) processes which result in cosine-form coherence when the lifetime of the excited electrons is much longer than the cycle of coherent phonons. In the TDFS and DECP processes, a pump pulse creates the real population of electrons in the conduction band and the ion-to-ion potentials are deformed. Coherent phonons are generated in the crystal which start to oscillate around new equilibrium positions. Totally symmetric phonon modes are excited in the DECP mechanism while LO phonon modes in the depletion layer are excited in the TDFS process by a transient change in the electrical surface field. The bandgap of rutile is larger than the pump photon energy used in our study. The electronic resonance between occupied midgap states and the conduction band is needed to enable the resonant ISRS, TDFS, and DECP. The vacuum-prepared rutile wafers contain oxygen-atom vacancies accompanied by Ti^{3+} cations. The d-electrons localized on the Ti^{3+} ions possibly provide occupied midgap states. The occupied midgap states derived from the Ti^{3+} ions also can contribute to the nonoscillatory SH decay components. A trapping of photoexcited electrons and a transport of photoexcited holes can result in a change in SH efficiency after photoexcitation from occupied midgap states to conduction band.

B. Assignment of third-order response

The $\chi^{(3)}$ responses of the A_{1g} phonon mode at 610 cm^{-1} were successfully fitted with $\theta_\nu=0$ in the [001]sp, [1$\bar{1}$0]sp, and [1$\bar{1}$0]pp spectra. This indicates that the ISRS process excites that mode. The other band at 200 cm^{-1} is rather cosinelike with $\theta_\nu=62$ suggesting some contribution of the electronic resonance.

C. Assignment of fourth-order responses

Third-order response is bulk sensitive in rutile with centrosymmetry. On the other hand, fourth-order response is interface sensitive. Here, we estimate the thickness of the surface layer observable by the $\chi^{(4)}$ response. The $\chi^{(4)}$ response is produced in a finite portion of the centrosymmetric TiO₂ medium because of the upward band bending from the bulk to the surface. The band bending of the surface depletion layer in TiO₂ was reported as electric field induced SH intensity dependence in electrochemical treatment.[28] The thickness of the $\chi^{(4)}$-sensitive portion depends on the concentration of surface electronic states and donor states. The observable thickness is practically determined by the escape depth of the SH light. By considering the refractive index at the SH wavelength, $\kappa=2$ at 310 nm,[29] the observable depth is estimated to be 10 nm.

Now we start to assign the seven $\chi^{(4)}$ bands. Rutile bulk structure is in D_{4h}^{14} symmetry. When a rutile crystal is truncated with a plane perpendicular to the [110] direction, the fourfold axis is lost to yield C_{2v} symmetry. Table [III] shows the relationship of the irreducible representation in D_{4h} and C_{2v} symmetry groups. The corresponding Raman tensor components and pump light polarization in our experiments are listed together. Here, the z axis is in the [110] direction with x axis parallel to the [001] direction.

The lowest wave number band at 179 cm^{-1} appeared only in the [001]pp spectrum with $\theta_\nu=0$. The zero phase suggests the ISRS mechanism in the coherent excitation. The irreducible representation only related to the [001]p Raman pump is B_1 on the surface according to Table [III]. When a bulk phonon is projected to a B_1 surface mode, the bulk mode should exhibit A_{2u}, B_{2u}, or E_g symmetry. A transverse optical A_{2u} mode [Fig. [3(a)]] was found at 167 cm^{-1} in bulk rutile[22] with the closest wave number. We thus assign the $\chi^{(4)}$ band at 179 cm^{-1} to the A_{2u} (TO) phonon projected on the (110) surface. The wave number of the bulk mode shifts by +12 cm^{-1} on the surface.

Two $\chi^{(4)}$ bands at 191 and 507 cm^{-1} are assigned in a
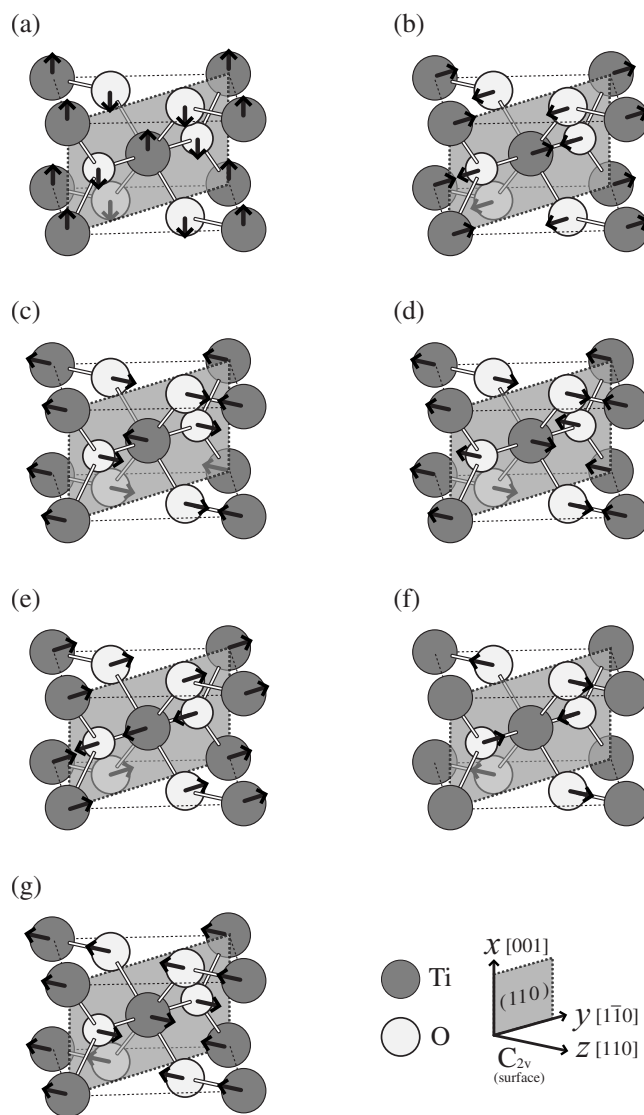

FIG. 3. Atomic displacements of the corresponding bulk phonon modes of the observed surface modes after Ref. [22]. (a) A_{2u} (TO: 167 cm^{-1}) mode that was observed as B_2 mode at 179 cm^{-1}. (b) One of E_u (TO: 183 cm^{-1}) modes that corresponds to B_2 mode observed at 191 cm^{-1}. (c) One of E_u (LO: 373 cm^{-1}) modes observed as A_1 mode at 359 cm^{-1}. (d) One of E_u (LO: 458 cm^{-1}) modes observed as A_1 mode at 440 cm^{-1}. (e) One of E_u (TO: 500 cm^{-1}) modes observed as B_2 mode at 507 cm^{-1}. (f) A_{1g} (612 cm^{-1}) mode observed as A_1 mode at 609 cm^{-1}. (g) One of E_u (LO: 807 cm^{-1}) modes.

TABLE III. Correspondences of original irreducible representations of D_{4h} (bulk TiO$_2$), irreducible representations of C_{2v} [TiO$_2$ (110) surface], and possible pump polarizations.

Original point group D_{4h}	Point group on surface			Input pulse direction and pump polarization (possible pump polarization)
	C_{2v}	transformation	properties	
$A_{1g}B_{1g}E_u$	A_1	$z[110]$	x^2, y^2, z^2	$[001]p(z^2, x^2)$, $[001]s(y^2)$, $[1\bar{1}0]p(z^2, y^2)$, $[110]s(x^2)$
$A_{1u}B_{1u}E_g$	A_2		xy	
$A_{2u}B_{2u}E_g$	B_1	$x[001]$	xz	$[001]p(xz)$
$A_{2g}B_{2g}E_u$	B_2	$y[1\bar{1}0]$	yz	$[1\bar{1}0]p(yz)$

similar way. Each mode is related to one of degenerated E_u (TO) mode with B_2 symmetry on the surface [Figs. 3(b) and 3(e)]. They are pumped by the ISRS mechanism and the wave number shifts from the bulk to the surface were +8 and +7 cm^{-1}, respectively.

A $\chi^{(4)}$ response at 609 cm^{-1} appeared in the [001]sp spectrum. It is related to an A_{1g} bulk phonon at 612 cm^{-1} [Fig. 3(f)] because of the correspondence of wave numbers and the excitation symmetry. This bulk mode is responsible for the $\chi^{(3)}$ response at 610 cm^{-1}. The nonzero phase of the $\chi^{(4)}$ response suggests an electronic excitation contributing the coherent excitation. The A_{1g} mode is projected to an A_1 mode on the surface and the A_1 mode excitation is allowed with the [001]s, [001]p, [1\bar{1}0]s, and [1\bar{1}0]p pump polarizations. The band actually appeared in the [001]sp spectrum, while being absent in the other three spectra for an unknown reason.

Three $\chi^{(4)}$ bands appeared in the [001]pp spectrum at 368, 440, and 817 cm^{-1}. They are present also in the [001]sp, [1\bar{1}0]pp, and [1\bar{1}0]sp spectra with one exception of the 440 cm^{-1} band in the [001]sp spectrum. The perfect and nearly perfect appearances with the different azimuths and

polarizations suggest A_1 symmetry of the three surface phonon modes. The corresponding bulk modes are A_{1g}, B_{1g}, or E_u as seen in Table III. According to Table II of Ref. 22, two E_u (LO) phonons are present at 373 and 458 cm^{-1}. We assigned the $\chi^{(4)}$ band at 368 and 440 cm^{-1} to the two E_u (LO) modes with wave number shifts of −5 and −18 cm^{-1}, respectively [Figs. 3(c) and 3(d)].

The last $\chi^{(4)}$ band exhibited wave numbers ranging from 817 to 827 cm^{-1} in the four spectra. In our previous paper[10] the $\chi^{(4)}$ band was assigned to the B_{2g} mode due to close wave numbers. However B_{2g} is not corresponding to A_1 symmetry. On the other hand, the E_u (LO) mode of 807 cm^{-1} [Fig. 3(g)] presents an intense hyper-Raman band at 822 cm^{-1} (Ref. 30) and corresponding to A_1 symmetry. Hence we now propose a contribution of the E_u (LO) mode as the origin of the $\chi^{(4)}$ band at 817−827 cm^{-1}.

In a viewpoint of the hyper-Raman process, which is the probe process of the measurement, A_1 and B_1 symmetries are symmetrically allowed in the results of [001] azimuth while A_1 and B_2 symmetries are allowed in the results of [1\bar{1}0] azimuth when p-polarized probe pulses were used. Selective observation of the B_1 and B_2 modes may be possible by

TABLE IV. Frequency and assignment of phonon modes observed in (a) fourth-order spectra and (b) third-order spectra.

(a) Fourth-order Raman

Crystal orientation, input polarization, and observed frequency (cm^{-1})				Assignment and k-vector direction	Corresponding bulk mode and reported frequency[a] (cm^{-1})
[001]pp	[001]sp	[1\bar{1}0]pp	[1\bar{1}0]sp		
179	⋯	⋯	⋯	B_1 (TO) in (001)	A_{2u} (TO), 167
⋯	⋯	191	⋯	B_2 (TO) in (1\bar{1}0)	E_u (TO), 183
368	368	365	359	A_1 (LO), [110]	E_u (LO), 373
440	⋯	443	440	A_1 (LO), [110]	E_u (LO), 458
⋯	⋯	507	⋯	B_2 (TO) in (1\bar{1}0)	E_u (TO), 500
⋯	609	⋯	⋯	A_1 in (1\bar{1}0)	A_{1g}, 612
817	827	827	823	A_1 (LO), [110]	E_u (LO), 807

(b) Third-order Raman

Crystal orientation, input polarization, and observed frequency (cm^{-1})				Assignment
[001]pp	[001]sp	[1\bar{1}0]pp	[1\bar{1}0]sp	
201	⋯	⋯	⋯	Overtones or combinations
⋯	615	607	614	A_{1g}

[a]Reference 22.

using *s*-polarized probe pulses. However, on our TiO$_2$ wafers the SH intensity was small with the *s*-polarized probe pulses. It was difficult to examine the B_1 and B_2 modes.

D. Contribution of the non-ISRS mechanisms in LO modes

The phase of the three $\chi^{(4)}$ bands at around 359, 440, and 823 cm^{-1} is sensitive to the azimuths and polarizations. In the [001]pp spectrum, their phases were close to zero. Hence, a dominant contribution of the ISRS is expected to produce the $\chi^{(4)}$ response. On the other hand, those bands presented phases far from zero when pumped with *s*-polarized pulses. As we assigned the three modes at 359, 440, and 823 cm^{-1} to A_1 derived from bulk E_u (LO), the phonon vibrations in the three modes are the polar modes toward the surface normal [Figs. 3(c), 3(d), and 3(g)] and they can be sensitive to the depletion field. Hence a definite contribution of the TDFS mechanism was assumed in order to interpret the *s*-polarized pump results. For excitation of coherent phonons of TiO$_2$ in TDFS, we assumed photoexcitation from an occupied mid-gap state derived from the Ti^{3+} to the conduction band.

The azimuths and polarization dependences of the phases can be explained by different ratios of excitation efficiencies in ISRS and non-ISRS mechanisms. It is natural that the amplitude of Raman tensor components is sensitive to polarizations. The fraction of the ISRS is dominant in the [001]pp spectrum, medium in the [1$\bar{1}$0]pp spectrum, and small in the [001]sp and [1$\bar{1}$0]sp spectra. The ISRS excitation together with TDFS has been reported in coherent phonon excitation in zinc-blende semiconductors.[31]

The different bandwidths of 359, 440, and 823 cm^{-1} bands suggest different excitation mechanisms. The bandwidth of 359 cm^{-1} was narrower than those of the other modes. The displacements of Ti atoms are in the opposite direction to the displacements of the O atoms in the mode at 359 cm^{-1}, as illustrated in Fig. 3(c). When a depletion field appears at the surface, that mode can be efficiently excited.

With a homogeneous broadening assumption, the dephasing time of the 440 and 823 cm^{-1} bands is 1 ps. The nonoscillatory decay of the raw SH intensity was fitted with time constants of 0.16 and 1.2 ps in Fig. 2. The two characteristic times agreed at 1 ps. The excited-state electron dynamics may possibly affect the lifetime of the coherent phonons at 440 and 823 cm^{-1} via the DECP mechanism.

The assignments of the $\chi^{(3)}$ and $\chi^{(4)}$ responses are summarized in Table IV. The atom displacements in the corresponding bulk phonon modes are illustrated in Fig. 3 following a theoretical study by Lee *et al.*[22] The $\chi^{(4)}$ response of a Raman-active mode of vibration is enhanced when the Raman transition is in resonance with a one-photon electronic transition. This happened on an oxazin dye solution,[12] where Raman-active bands were observed. On the other hand, the pump photon energy is out of resonance in the present study and infrared-active modes of the bulk crystal appeared in the $\chi^{(4)}$ responses as a result of two-photon resonance of the probing hyper-Raman process. These results offer selective

observation of $\chi^{(4)}$ responses originated from Raman-active and infrared-active modes by tuning the pump photon energy.

V. SUMMARY

The fourth-order optical responses of a wide-bandgap material, rutile TiO$_2$, were observed by a pump-and-probe method with different azimuths and polarizations of pump and probe light pulses. The observed responses were assigned to seven phonon modes present in the surface layer of 10 nm thickness. Possible contributions of the ISRS and TDFS are evaluated on each $\chi^{(4)}$ response. It was suggested that Raman-active and infrared active phonon modes can be selectively observed in a wide-bandgap material by tuning the pump photon energy.

[1] R. Fuchs and K. L. Kliewer, Phys. Rev. **140**, A2076 (1965).
[2] H. Ibach, Phys. Rev. Lett. **24**, 1416 (1970); L. L. Kesmodel, J. A. Gates, and Y. W. Chung, Phys. Rev. B **23**, 489 (1981); G. Rocker, J. A. Schaefer, and W. Göpel, *ibid.* **30**, 3704 (1984); P. A. Cox, R. G. Egdell, S. Eriksen, and W. R. Flavell, J. Electron Spectrosc. Relat. Phenom. **39**, 117 (1986); M. A. Henderson, Surf. Sci. **355**, 151 (1996); H. Ibach and D. L. Mills, *Electron Energy Loss Spectroscopy and Surface Vibrations* (Academic, New York, 1982).
[3] R. G. Greenler, J. Chem. Phys. **44**, 310 (1966); F. M. Hoffmann, Surf. Sci. Rep. **3**, 107 (1983); Y. J. Chabal, *ibid.* **8**, 211 (1988).
[4] J. P. Toennies, J. Vac. Sci. Technol. A **5**, 440 (1987).
[5] Y. R. Shen, *The Principles of Nonlinear Optics* (Wiley, New York, 1984); Y. R. Shen, Nature (London) **337**, 519 (1989); K. B. Eisenthal, Chem. Rev. (Washington, D.C.) **96**, 1343 (1996); T. Ishibashi and H. Onishi, Appl. Phys. Lett. **81**, 1338 (2002); T. Ishibashi and H. Onishi, Appl. Spectrosc. **56**, 1298 (2002); J. E. Patterson, A. Lagutchev, W. Huang, and D. D. Dlott, Phys. Rev. Lett. **94**, 015501 (2005); A. Lagutchev, S. A. Hambir, and D. D. Dlott, J. Phys. Chem. C **111**, 13645 (2007).
[6] T. Ishibashi, H. Uetsuka, and H. Onishi, J. Phys. Chem. B **108**, 17166 (2004).
[7] Y. Matsumoto and K. Watanabe, Chem. Rev. (Washington, D.C.) **106**, 4234 (2006).
[8] U. Bovensiepen, A. Melnikov, I. Radu, O. Krupin, K. Starke, M. Wolf, and E. Matthias, Phys. Rev. B **69**, 235417 (2004); Y. M. Chang, L. Xu, and H. W. K. Tom, Phys. Rev. Lett. **78**, 4649 (1997); K. Watanabe, N. Takagi, and Y. Matsumoto, Chem. Phys. Lett. **366**, 606 (2002).
[9] Y. M. Chang, H. H. Lin, C. T. Chia, and Y. F. Chen, Appl. Phys. Lett. **84**, 2548 (2004).
[10] S. Fujiyoshi, T. Ishibashi, and H. Onishi, J. Phys. Chem. B **109**, 8557 (2005).
[11] S. Fujiyoshi, T. Ishibashi, and H. Onishi, J. Phys. Chem. B **110**, 9571 (2006).
[12] S. Fujiyoshi, T. Ishibashi, and H. Onishi, J. Phys. Chem. B **108**, 10636 (2004).
[13] Y. Hirose, H. Yui, and T. Sawada, J. Phys. Chem. B **109**, 13063 (2005).
[14] S. Yamaguchi and T. Tahara, J. Phys. Chem. B **109**, 24211 (2005).
[15] T. Nomoto and H. Onishi, Chem. Phys. Lett. **455**, 343 (2008).
[16] S. Yamaguchi and T. Tahara, Angew. Chem., Int. Ed. **46**, 7609 (2007).
[17] T. Nomoto and H. Onishi, Phys. Chem. Chem. Phys. **9**, 5515 (2007); Appl. Spectrosc. **63**, 941 (2009).
[18] H. Sano, G. Mizutani, W. Wolf, and R. Podloucky, Phys. Rev. B **70**, 125411 (2004); M. Omote, H. Kitaoka, E. Kobayashi, O. Suzuki, K. Aratake, H. Sano, G. Mizutani, W. Wolf, and R. Podloucky, J. Phys.: Condens. Matter **17**, S175 (2005).
[19] W. G. Spitzer, R. C. Miller, D. A. Kleinman, and L. E. Howarth, Phys. Rev. **126**, 1710 (1962); D. M. Eagles, J. Phys. Chem. Solids **25**, 1243

(1964).

[20] S. P. S. Porto, P. A. Fleury, and T. C. Damen, Phys. Rev. **154**, 522 (1967).

[21] J. G. Traylor, H. G. Smith, R. M. Nicklow, and M. K. Wilkinson, Phys. Rev. B **3**, 3457 (1971).

[22] C. Lee, P. Ghosez, and X. Gonze, Phys. Rev. B **50**, 13379 (1994).

[23] J. H. Nicola, C. A. Brunharoto, M. Abramovich, and C. E. T. Conçalves da Silva, J. Raman Spectrosc. **8**, 32 (1979).

[24] T. Pfeifer, T. Dekorsy, W. Kütt, and H. Kurz, Appl. Phys. A: Mater. Sci. Process. **55**, 482 (1992).

[25] H. J. Zeiger, J. Vidal, T. K. Cheng, E. P. Ippen, G. Dresselhaus, and M. S. Dresselhaus, Phys. Rev. B **45**, 768 (1992).

[26] G. A. Garrett, T. F. Albrecht, J. F. Whitaker, and R. Merlin, Phys. Rev. Lett. **77**, 3661 (1996).

[27] T. E. Stevens, J. Kuhl, and R. Merlin, Phys. Rev. B **65**, 144304 (2002); D. M. Riffe and A. J. Sabbah, *ibid.* **76**, 085207 (2007).

[28] J. M. Lantz, R. Baba, and R. M. Corn, J. Phys. Chem. **97**, 7392 (1993).

[29] M. Cardona and G. Harbeke, Phys. Rev. **137**, A1467 (1965).

[30] V. N. Denisov, B. N. Mavrin, V. B. Podobedov, and K. E. Sterin, Opt. Commun. **34**, 357 (1980).

[31] K. J. Yee, Y. S. Lim, T. Dekorsy, and D. S. Kim, Phys. Rev. Lett. **86**, 1630 (2001); Y. M. Chang, Appl. Phys. Lett. **82**, 1781 (2003); K. Ishioka, M. Kitajima, J. Irisawa, Y. Hironaka, K. Ushida, and K. G. Nakamura, Jpn. J. Appl. Phys., Part 1 **45**, 9111 (2006).